Available online at www.sciencedirect.com
SCIENCE DIRECT®
Polymer 45 (2004) 1951–1957
polymer
www.elsevier.com/locate/polymer

Rod–rod and rod–coil self-assembly and phase behavior of polypeptide diblock copolymers

Elizabeth A. Minich[a], Andrew P. Nowak[b], Timothy J. Deming[b], Darrin J. Pochan[a,*]

[a]*Department of Materials Science and Engineering, Delaware Biotechnology Institute, University of Delaware, 201 DuPont Hall, Newark, DE 19716, USA*
[b]*Departments of Materials and Chemistry, University of California at Santa Barbara, Santa Barbara, CA 93106, USA*

Received 21 August 2003; received in revised form 21 December 2003; accepted 9 January 2004

Abstract

Poly(γ-benzyl L-glutamate) (PBLG) forms a rigid helical rod in organic solvents. Cholesteric liquid crystalline ordering of these rods has been observed in PBLG solutions and cast films. In this research, peptidic block copolymers were created using PBLG in order to determine the effect of an added block on the classic cholesteric ordering. Peptide blocks with varied lengths and inherent secondary structures, random coil or rigid rod, were attached to PBLG molecules. The self assembly/liquid crystalline ordering of these molecules in films cast from various organic solvents was probed with transmission electron microscopy (TEM), atomic force microscopy (AFM), and X-ray diffraction (XRD). In pure PBLG and PBLG diblock copolymers with relatively small additional blocks, cholesteric liquid crystalline ordering was observed in bulk films. However, depending on the kinetics of film formation and the amount of non-PBLG block, significant changes in the nanostructure and microstructure were observed. These purely peptidic block molecules provide the opportunity to pattern materials with peptidic functionalities by taking advantage of block copolymer phase behavior and liquid crystal ordering.

Keywords: PBLG; Polypeptide; Block copolymers

1. Introduction

The ability to pattern materials from the nano- to microscale plays an important role in biological applications, such as tissue engineering and cellular biosensors. For example, soft lithography, based on replica molding self-assembly, is a useful technique for biological applications [1,2]. Micropatterned substrates produced by soft lithography have provided precise control of cellular position and function on surfaces, which is essential for the fabrication of biosensors, bioreactors, and other biofunctional materials [3,4]. Non-lithographic techniques for producing ordered materials include molecular self-organization based on competing interactions. The use of synthetic homo- and block copolymers to produce ordered, functional materials has been widely investigated [5–11]. Using block copolymer and comb copolymer systems, these techniques traditionally form nano-scale spherical, cylindrical, cubic, and lamellar structures in the bulk [5–8]. Thin film templates have been created when block copolymers spontaneously self-organize into nano-scale patterns over large surface areas of desired substrates [9–11]. Self-assembly in liquid crystalline systems can also be used to form nano- to microscale structure useful in responsive applications. For example, liquid crystals have been used to create tunable structures, such as switches and dyes, used in electronic, optical, and magnetic materials [12,13]. The work on model diblock copolypeptides described herein attempts to use facets of liquid crystalline, block copolymer, and biopolymer materials to form hierarchically ordered materials with biofunctionality.

Molecular architecture and polymer secondary structure significantly effect the self-assembly and phase behavior of block copolymer-based materials [14–20]. Because of its α-helical secondary structure, poly(γ-benzyl L-glutamate) (PBLG) forms a rigid rod and exhibits liquid crystalline ordering in concentrated solutions and cast films. PBLG, a commercially available liquid crystalline polymer since the 1950's [21], has been used as a model rigid rod system in studying gelation and rheological properties in order to solve industrial liquid crystal polymer processing problems

* Corresponding author. Tel.: +1-302-831-3569; fax: +1-302-831-4545.
E-mail address: pochan@udel.edu (D.J. Pochan).

0032-3861/$ - see front matter © 2004 Published by Elsevier Ltd.
doi:10.1016/j.polymer.2004.01.009

[22–26]. Liquid crystalline polymers have local orientational order that provides for several desirable material characteristics, including superior mechanical properties, thermal stability, and chemical resistance [27]. These polymers also provide the opportunity to pattern materials with peptidic functionalities by taking advantage of the liquid crystalline ordering of block copolypeptides containing PBLG.

Two types of liquid crystalline order are observed in PBLG systems. Smectic layering is observed in solutions and films of monodisperse PBLG rods synthesized using recombinant DNA techniques [28,29]. However, when molecular irregularity is introduced to the system, the smectic structure is disturbed and cholesteric order is seen. Cholesteric liquid crystalline ordering is predominantly observed in concentrated solutions and cast films of PBLG with a greater degree of polydispersity [21,30] or with the addition of a second block [31–35]. This twisting nematic phase was initially found in cholesterol derivatives, hence the name 'cholesteric' [36]. The cholesteric structure occurs with rigid, chiral molecules and has been observed in several polypeptides with an α-helical conformation, such as poly-γ-ethyl-L-glutamate (PELG) and poly-β-benzyl-L-aspartate (PBLA) [37]. The cholesteric phase is composed of a twisting stack of nematically ordered molecular planes that arises from the helical nature of the PBLG rods. As one nematic plane is slightly skewed from the plane above, a periodic superstructure is formed characterized by the pitch. In solutions, left or right handedness of the pitch depends on the dielectric constant of the solvent [30]. The magnitude of the pitch fluctuates with temperature and has become a useful feature in making thermometers [36]. In solid films, where little or no solvent is present, the pitch is on the order of 1 μm [21]. Polarizing optical microscopy (POM), TEM, and AFM reveal regularly spaced retardation lines, defined as 1/2 the pitch that form a fingerprint pattern. These patterns contain characteristic liquid crystalline defects, such as π-disclinations and edge dislocations [38,39].

The assembly and phase behavior of synthetic diblock copolymers consisting of a rigid block coupled to a flexible block has been well studied. These copolymers have been shown to exhibit a variety of micro and nano phase-separated morphologies depending on the total degree of polymerization, the volume fraction of the blocks, and the incompatibility between the blocks (Flory–Huggins interaction parameter, χ_{AB}). The stiffness of the rod segment causes the polymers to assemble into anisotropic liquid crystalline phases that can be controlled by temperature and solvent concentration [17–20]. Compared to rod–rod block copolymers, rod–coil block copolymers have a relatively high Flory–Huggins interaction parameter because of the conformational asymmetry between the rod and coil segments [14,31,40,41].

Although PBLG block copolymer systems have previously been reported [31–35], our copolymers are unique in that they are completely peptidic. This provides the opportunity to pattern materials exclusively with peptidic functionality. Our study investigates the bulk phase behavior of rod or coil peptidic block addition to the rigid PBLG rod. We have found that PBLG diblock copolymers with non-PBLG block addition of up to 50% by volume continue to exhibit cholesteric ordering, depending on the kinetics of film formation. However, when a solvent with a high vapor pressure was used to cast the film, significant changes in the microstructure of PBLG with a large added block were observed. In addition, clear local hexagonal packing was seen in films cast with a low vapor pressure solvent.

2. Experimental

2.1. Materials

All block copolypeptides were synthesized according to published procedures [42,43]. While secondary structure was not explicitly investigated in this paper, the conformational behavior of the polypeptides studied herein is well documented. Data to support the proposed random coil and rod-like structure of the blocks can be found in Nowak et al. [43] and Yu et al. [44], respectively. Molecular characteristics of the series studied here are listed in Table 1.

2.2. Film preparation

Bulk films with a thickness of approximately 1 mm were cast in glass beakers by thoroughly dissolving the peptides in pentachloroethane, chloroform, or DMF solvent and allowing slow solvent evaporation over several days. Selective solvent studies were done using DMF, a good solvent for the PBLG block. Samples were subsequently placed in a vacuum oven at 50 °C overnight to remove the remaining solvent.

2.3. Polarizing optical microscopy

A drop of ~40 wt% PBLG block copolypeptide solution was placed on a glass slide. The sample was viewed between crossed polarizers using a Nikon Microphot-SA optical microscope.

2.4. Transmission electron microscopy

The dried bulk films were microtomed both parallel and perpendicular to the film surface. Sections with a thickness of ~80 nm were cut at room temperature without embedding using a Leica Ultracut UCT and a diamond knife. The sections were placed on copper grids, stained with RuO_4 for 5 min, and carbon coated. TEM bright field imaging was preformed with at JOEL 2000FX microscope at an accelerating voltage of 200 kV.

Table 1
List of characterization data for block copolymers used. N is defined as the number of monomers in the respective block, f_{BLOCK} is the mole fraction of the added block, and W_i is the weight fraction of the added block

Sample	Block conformation [43,44]	M_n[a] (g/mol)	M_w/M_n[b]	N_{PBLG}	N_{BLOCK}	f_{BlOCK}[a]	W_i
$PBLG_{100}$	–	22,000	1.2	100	0	0.00	–
$PBLG_{90}L_{10}$	Rod	21,000	1.2	90	10	0.10	0.05
$PBLG_{80}L_{20}$	Rod	20,000	1.2	80	20	0.20	0.11
$PBLG_{80}(LV)_{20}$	Loose rod	20,000	1.2	80	20	0.20	0.11
$PBLG_{75}racL_{75}$	Random coil	26,000	1.2	75	75	0.50	0.33

[a] Estimated from momomer initiator ratios.
[b] Measured using a Wyatt DAWN SEC/light scattering detector.

2.5. Atomic force microscopy

Dried films were microtomed perpendicular to the film surface at a thickness of 1 μm and placed on a silicon wafer fixed to an AFM mount. Amplitude (derivative of topology signal) images were collected with a Nanoscope IIIa Atomic Force Microscope in tapping mode and a Nanodevices TAP300 tip.

2.6. X-ray diffraction

XRD data shown in Fig. 2 were collected in transmission mode on a pinhole-collimated camera equipped with a Rigaku copper target rotating anode ($\lambda = 1.54$ Å) operated at 3.6 kW and a Bruker, 2-dimensional detector. XRD experiments shown in Figs. 4 and 5 were performed in transmission mode at the National Synchrotron Light Source (NSLS) at Brookhaven Laboratory on beamline X10A ($\lambda = 1.55$ Å, $E = 8$ keV). The film surface was perpendicular to the beam path. Data were collected using a Bruker CCD detector and integrated into one-dimensional plots of intensity versus scattering vector, q, where $q = (4\pi/\lambda)\sin(\theta)$ and θ is the Bragg angle (or 1/2 the scattering angle).

3. Results and discussion

Block copolymers, listed in Table 1, were designed in order to determine the effects of block addition on the classic PBLG cholesteric phase behavior. Leucine (L), racemic copolymers of L and D leucine (racL), or a random copolymer of L and valine (V) blocks with the inherent secondary structures of random coil (racL or LV) or rigid rod (L), were attached to PBLG molecules. The phase behavior was controlled by altering the block's secondary structure and length relative to the PBLG block.

Polarizing optical microscopy (POM) shows birefringence in concentrated solutions (~40 wt%) of PBLG and PBLG-peptide block copolymers in pentachloroethane, chloroform, and DMF. Birefringence occurs from the anisotropic nature of nematically-ordered molecules and has been observed in PBLG solutions of high concentration [29,45].

The ordering of these molecules in bulk films cast from organic solvent was probed with TEM. Fig. 1 shows microtomed sections of bulk PBLG films cast from pentachloroethane, a good solvent for both blocks with a low vapor pressure that guaranteed films were slowly cast from homogeneous solution. Sections cut parallel and perpendicular to the film surface show similar features, indicating that the bulk films have an isotropic macrostructure. The appearance of a lamellar structure observed in the TEM images suggests cholesteric twisting of the PBLG homopolymer and PBLG copolymers with up to 50%

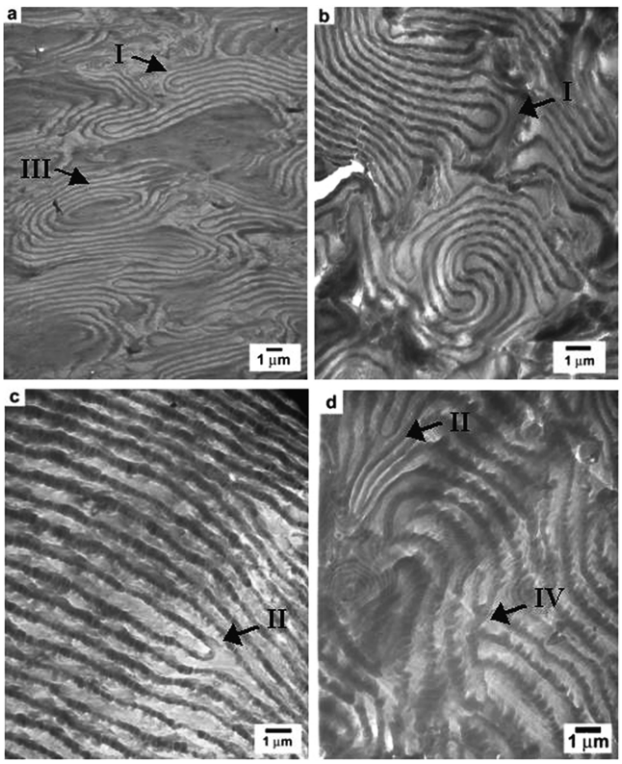

Fig. 1. TEM bright field images of microtomed films cast in pentachloroethane. $PBLG_{100}$ cut (a) parallel and (b) perpendicular to the film surface show isotropy of the bulk film. (c) $PBLG_{80}L_{20}$ and (d) $PBLG_{75}racL_{75}$ cut perpendicular to the film surface. Characteristic liquid crystalline defects are indicated by (I) + π and (II)-π disclinations, (III) the helix ring morphology, and (IV) a T-junction.

random coil block addition. Alternating dark and light bands correlate to the twist of molecular orientation in the cholesteric phase, as seen in previously reported systems [28,38,39,46–49]. This banding reveals retardation lines, defined as 1/2 the cholesteric pitch. The size of the pitch observed in the images can vary depending on the orientation of the cholesteric axis in the plane of the microtomed sections. In the PBLG homopolymer, the pitch is on the order of 1 μm when the cholesteric axis is oriented approximately in the plane of the microtomed section. This value agrees with PBLG pitch size reported previously [21]. Dark regions where no banding is seen correspond to areas viewed down the cholesteric axis when it is aligned perpendicularly to the plane of the image. Characteristic liquid crystalline defects, denoted I–IV, can be seen in the TEM images. A fingerprint pattern is created by π-disclinations [38,39] and the helix ring morphology [46]. T-junction boundaries, discussed by Gido and Thomas [50], are also observed and can be attributed to stresses during the film casting process.

Fig. 2 shows XRD curves of films cast from the pentachloroethane. The intense peak with a *d*-spacing of 13.2 Å corresponds to the distance between the (10) plane of hexagonally packed PBLG rods. A set of Bragg peaks with a wave vector ratio of $q_1 : \sqrt{3}q_1 : 2q_1$ is observed that indicates a two-dimensional columnar hexagonal packing of the PBLG rods. The broad peak with a *d*-spacing of ~4 Å corresponds to a combination of the helical pitch [31] and the hydrocarbon chain diameter [51]. Local hexagonal packing of PBLG rods in the cholesteric phase has been proposed by Robinson et al. [45]. Columnar hexagonal

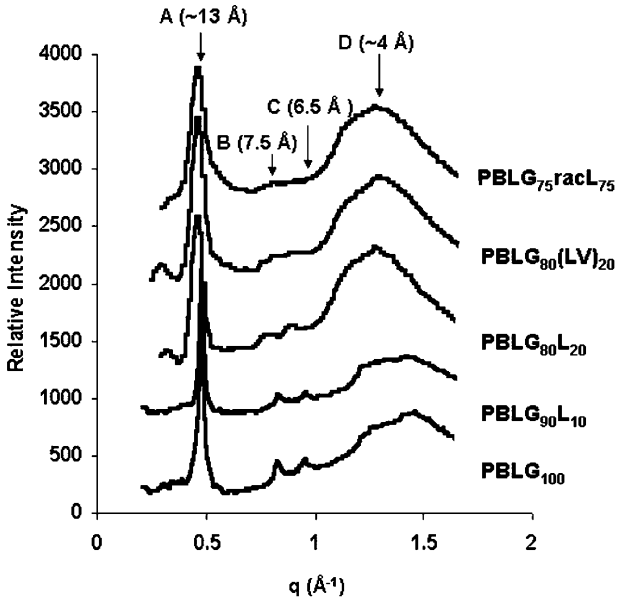

Fig. 2. XRD patterns of $PBLG_{100}$ and PBLG-block films cast in pentachloroethane. Peak A has a *d*-spacing of 13.2 Å, corresponding to the distance between molecules. Peaks A, B, and C have *d*-spacings with a ratio of 1:√3:2, suggesting columnar hexagonal arrangement of the PBLG rods. Intensity values were normalized to the most intense peak and the curves were offset for clarity.

arrangement has also been seen in PBLG-polystyrene, PBLG-poly(L-lactic acid), and PBLG-poly(ethylene glycol) block copolymers [31,32,35]. Competition exists between cholesteric packing due to chirality and hexagonal order due to molecular rigidity in high concentrations of chiral, rod-like molecules. Only a very small angular displacement between neighboring helical rods is required to produce a macroscopically cholesteric structure, while preserving some hexagonal packing on the molecular level within twisting nematic layers [52,53]. No scattering peaks were observed in small angle X-ray experiments. Therefore, the coexistence of hexagonal packing and a cholesteric superstructure was verified. The XRD patterns show a slight variation in the position of Peak A with the length of the added peptidic block. The hexagonally ordered PBLG rods in the PBLG homopolymer and $PBLG_{90}L_{10}$ are packed more tightly with a (10) peak position at higher scattering angle than in the other copolymers. In addition, Peak A and the subsequent hexagonal peaks become broader when the added block length is greater than 10 amino acid monomers due to more disorder in the packing of the PBLG rods.

Cholesteric structure can also be seen in films cast from chloroform, shown in Fig. 3. Chloroform has a higher vapor pressure than pentachloroethane. Therefore, films shown in Fig. 3 were cast more rapidly than those cast using pentachloroethane. In films cast using chloroform, a small added block slightly disrupts the banding on the micron length-scale and increases the pitch without altering the

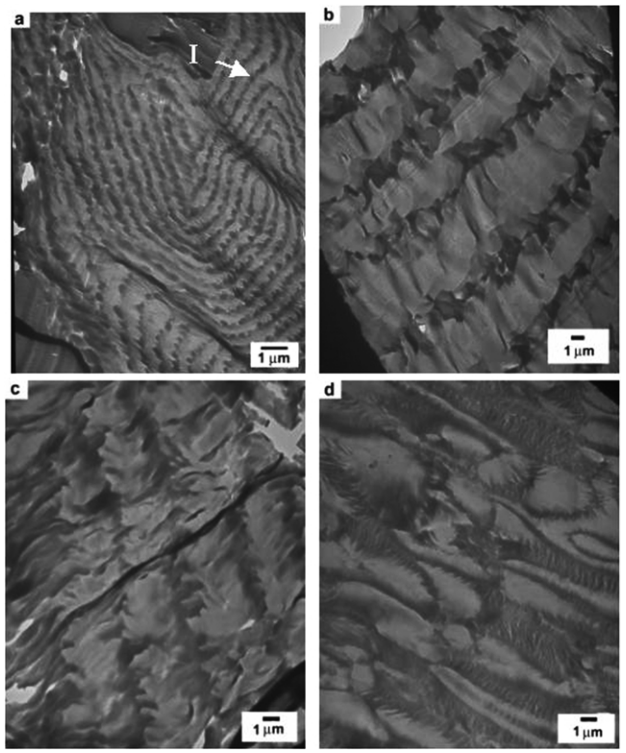

Fig. 3. TEM bright field images of microtomed films cast in chloroform and cut perpendicular to the bulk film surface. (a) $PBLG_{100}$, (b) $PBLG_{90}L_{10}$, (c) $PBLG_{80}(LV)_{20}$, and (d) $PBLG_{75}racL_{75}$. (I) denotes a -π disclination.

cholesteric nature of the ordering. This is shown in Fig. 3(b) and (c), in which the added block has a rod-like and random coil secondary structure, respectively. Banding is not seen in $PBLG_{75}racL_{75}$, which has a large random coil racemic leucine block that apparently prevents cholesteric arrangement.

Fig. 4 shows XRD curves of films cast using chloroform solvent. The intense peak with a *d*-spacing of 13 Å corresponds to the distance between nematically-ordered molecules in each plane of the cholesteric twist. Unlike the films cast in pentachloroethane, a set of Bragg peaks with a scattering angle ratio of $1{:}\sqrt{3}{:}2$ is not seen. The absence of columnar hexagonal packing in films cast from chloroform is attributed to the high vapor pressure of the solvent. Because chloroform evaporates more rapidly than pentachloroethane, the molecules have less time to order in a hexagonal fashion. In Fig. 4, the peaks at 13 Å are broader than in Fig. 2, indicating more disorder. Again, this is attributed to the high vapor pressure of the chloroform solvent relative to pentachloroethane in Fig. 2. The broad peak at ~4 Å in Fig. 4 corresponds to the helical pitch or the hydrocarbon chain diameter. No nano-scale differences are seen between the PBLG homopolymer and PBLG with additional blocks. $PBLG_{75}racL_{75}$ has a very different microstructure than the other molecules when observed in TEM but exhibits classic nematic order on the nano-scale.

Selective solvent studies using DMF, a good solvent for PBLG, do not show evidence of cholesteric banding in TEM images, Fig. 5(a). This featureless TEM data is representative of all the PBLG-X block copolymer films

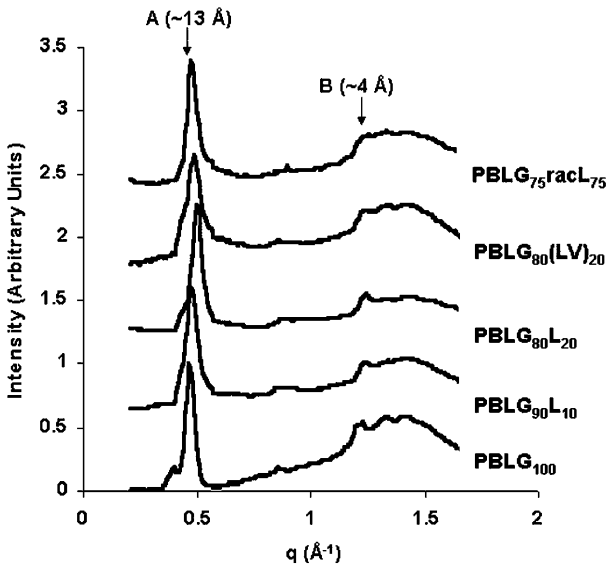

Fig. 4. XRD patterns of $PBLG_{100}$ and PBLG-block films cast in chloroform. Peak A has a *d*-spacing of ~13 Å, corresponding to the distance between nematically-ordered molecules. Peak B corresponds to the helical pitch and the hydrocarbon chain diameter. Intensity values were normalized to the most intense peak, and the curves were offset for clarity. A second order peak of A can be seen at ~0.9 $Å^{-1}$. The small peak shoulder on the side of Peak A at lower *q* is due to residual Kapton tape scattering that could not be subtracted from the data.

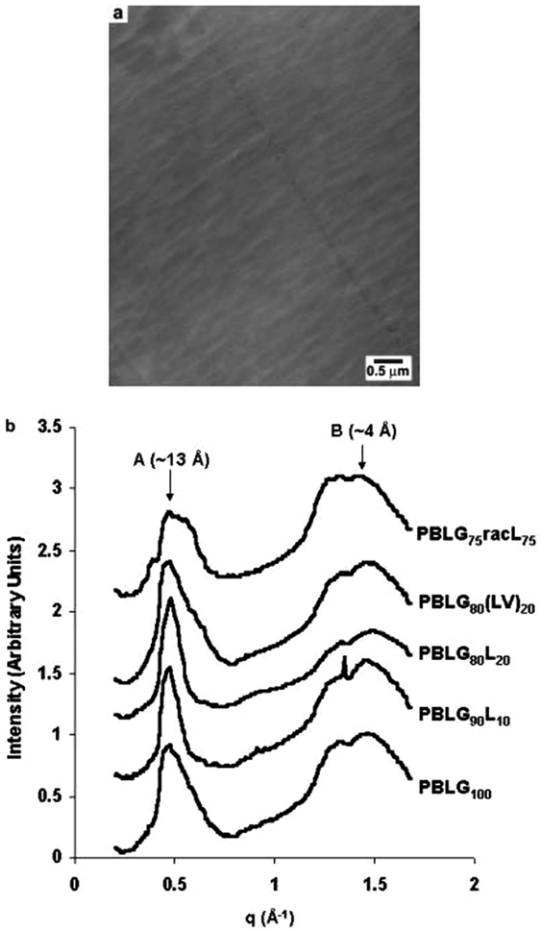

Fig. 5. (a) TEM bright field image of $PBLG_{100}$ film cast in DMF and microtomed perpendicular to the bulk film surface. (b) XRD patterns of $PBLG_{100}$ and PBLG-block films cast in DMF. Peak A has a *d*-spacing of ~13 Å, corresponding to the distance between nematically-ordered molecules. Peak B corresponds to the helical pitch and the hydrocarbon chain diameter. Intensity values were normalized to the most intense peak and the curves were offset for clarity. The small peak shoulder on the side of Peak A at lower q is due to residual Kapton tape scattering that could not be subtracted from the data.

cast from DMF. However, the XRD pattern in Fig. 5(b) is similar to the diffraction of films cast in chloroform, showing *d*-spacings of 13 and ~4 Å. This suggests that, although no cholesteric twisting structure is evident in the TEM images, the PBLG homopolymer and the PBLG block copolymers are nematically ordered. The broad first order scattering peak in Fig. 5(b) is due to a larger distribution of inter-rod spacing within the nematic phase compared to the spacing between molecules in the cholesteric samples. Due to significant disordering of the system, the inter-rod spacings are most broad and the least intense in the copolymers with larger additional coil blocks.

XRD data suggests all samples cast in chloroform and DMF have nematic order, while copolymers cast in pentachloroethane have local columnar hexagonal packing coexisting with cholesteric order. However, the addition of a

large random coil block to the PBLG rod results in an altered cholesteric structure depending on the solvent used. Fig. 6 shows TEM images of $PBLG_{75}racL_{75}$ microtomed sections cast in (a) pentachloroethane, (b) chloroform, and (c) DMF. Cholesteric ordering dominates in films cast from pentachloroethane due to the solvent's low vapor pressure. Slow evaporation over a period of a week allows for alignment of the PBLG rods, despite the presence of a 50% random coil block. Chloroform has more rapid evaporation over a period of a few days, which results in the absence of cholesteric structure in films. Like the PBLG homopolymer, no microstructure is seen in $PBLG_{75}racL_{75}$ films cast in DMF.

It has been proposed that observed TEM contrast in microtomed cholesteric phases is due to sample thickness variations [46–48]. AFM images of PBLG and PBLG diblock copolymer microtomed sections appear to have identical structure seen in TEM. Fig. 7 shows AFM amplitude images of $PBLG_{100}$ and $PBLG_{75}racL_{75}$. AFM suggests the light and dark bands seen in TEM images do, in fact, arise from a difference in sample thickness created by molecular orientation during sectioning. Thicker regions appear darker due to increased mass/thickness contrast. No significant shift in contrast was observed by tilting the specimen, again, indicating that most TEM contrast is due to sample thickness. Some contrast component might also exist from diffraction of the nematically oriented PBLG rods as they twist about the cholesteric axis. Dark and light bands appear depending on the strength of scattering when the molecules are aligned parallel or perpendicular to the electron beam [38,39,47,48]. However, direct observation of this molecular orientation-induced diffraction contrast is not possible due to the significant thickness differences in the microtomed samples.

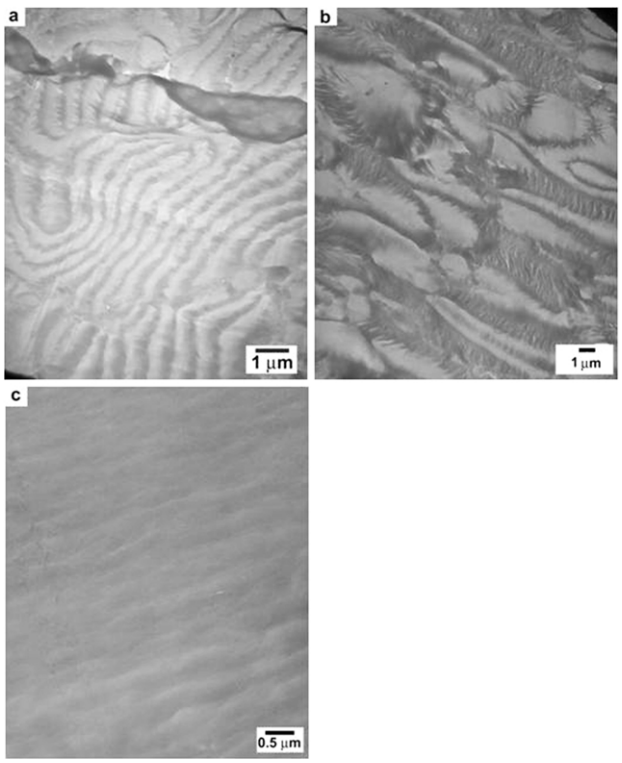

Fig. 6. TEM images of $PBLG_{75}racL_{75}$ microtomed sections cast in (a) pentachloroethane, (b) chloroform, and (c) DMF.

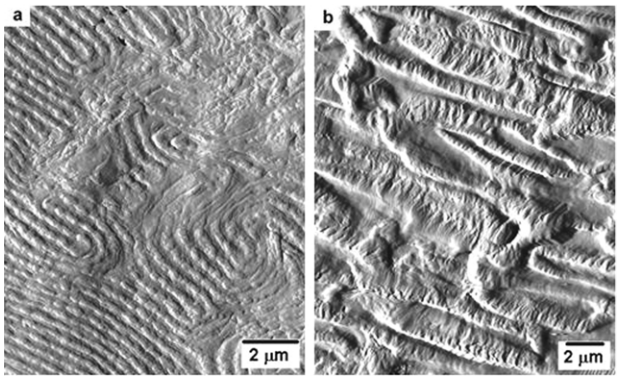

Fig. 7. AFM amplitude images of (a) $PBLG_{100}$ cast in pentachloroethane and (b) $PBLG_{75}racL_{75}$ cast in chloroform. These images mirror the TEM images in Figs. 1(b) and 3(d), indicating that the contrast seen in TEM is due to thickness fluctuations.

4. Conclusions

The phase behavior of PBLG-block copolymer bulk films cast in various solvents was investigated. TEM and XRD studies provide evidence of cholesteric order in PBLG homopolymer and PBLG with peptidic blocks. Characteristic cholesteric banding and defects were seen in films cast using pentachloroethane and chloroform solvents, but no banding was observed in films cast in DMF. Depending on the kinetics of film formation, significant changes in phase behavior were observed when the relative block length was increased. A slower rate of solvent evaporation allowed for improved cholesteric order. Unlike the copolymers with small blocks, a 50% random coil block in $PBLG_{75}racL_{75}$ prohibited the PBLG rods from having cholesteric structure in films cast in chloroform. However, cholesteric order was seen in $PBLG_{75}racL_{75}$ films cast in pentachloroethane. The low vapor pressure of pentachloroethane allowed for better molecular ordering compared to the other solvents. This is implied by local hexagonal packing of PBLG rods and the appearance of cholesteric banding in the sample with a large random coil block.

Cholesteric order is the dominant structure in PBLG-block films regardless of additional blocks up to 50 mol%. This diblock copolymer system creates a new approach for micro-scale patterning due to its chemical and topological ordered structure. A chemical pattern, determined by the cholesteric twist, could be created on the surface of microtomed films by adding functionalized groups the PBLG rod. The same ordered design exists in the topological features of the film, which can be used as a template for printing micro-scale patterns on a substrate.

Acknowledgements

This work was partially funded by the National Science Foundation under grant # CTS-9986347. Research carried out at the National Synchrotron Light Source, Brookhaven National Laboratory, is supported by the US Department of Energy, Division of Materials Sciences and Division of Chemical Sciences, under Contract No. DE-AC02-98CH10886. EAM and DJP acknowledge the University of Delaware College of Engineering W.M. Keck electron microscopy facility.

References

[1] Xia Y, Whitesides GM. Annu Rev Mater Sci 1998;28:153–84.
[2] Kane RS, Takayama S, Ostuni E, Ingber DE, Whitesides GM. Biomaterials 1999;20:2363–76.
[3] Chen CS, Mrksich M, Huang S, Whitesides GM, Ingber DE. Biotechnol Prog 1998;14:356–63.
[4] Chen CS, Mrksich M, Huang S, Whitesides GM, Ingber DE. Science 1997;276:1425–8.
[5] Kosonen H, Valkama S, Ruokolainen J, Knaapila M, Torkkeli M, Serimaa R, Monkman AP, ten Brinke G, Ikkala O. Synth Metals 2003; 137:881–2.
[6] Muthukumar M, Ober CK, Thomas EL. Science 1997;277:1225–32.
[7] Ruokolainen J, Makinen R, Torkkeli M, Makela T, Serimaa R, Brinke Gt, Ikkala O. Science 1998;280:557–60.
[8] Knaapila M, Ruokolainen J, Torkkeli M, Serimaa R, Horsburgh L, Monkman AP, Bras W, ten Brinke G, Ikkala O. Synth Metals 2001; 121:1257–8.
[9] Krausch G, Magerle R. Adv Mater 2002;14:1579–83.
[10] Leonard DN, Spontak RJ, Smith SD, Russell PE. Polymer 2002;43: 6719–26.
[11] Park M, Harrison C, Chaikin PM, Register RA, Adamson DH. Science 1997;276:1401–4.
[12] Kato T, Mizoshita N. Curr Opin Solid State Mater Sci 2002;6: 579–87.
[13] Lee S-W, Mao C, Flynn CE, Belcher AM. Science 2002;296:892–5.
[14] Pochan D, Gido SP, Zhou J, Mays JW, Whitmore M, Ryan AJ. J Polym Sci, Part B: Polym Phys 1997;35:2629–43.
[15] Chin L, Gido SP, Poulos Y, Hadjichristidis N, Tan NB, Trevino SF, Mays JW. Polymer 1998;39:4631–8.
[16] Avgeropoulos A, Dair BJ, Thomas EL, Hadjichristidis N. Polymer 2002;43:3257–66.
[17] Chen JT, Thomas EL, Ober CK, Mao G-P. Science 1996;273:343–6.
[18] Chen JT, Thomas EL, Ober CK, Hwang SS. Macromolecules 1995; 28:1688–97.
[19] Radzilowski LH, Stupp SI. Macromolecules 1994;27:7747–53.
[20] Li W, Gersappe D. Macromolecules 2001;34:6783–9.
[21] Samulski E. Liquid crystalline order in polypeptides. In: Blumstein A, editor. Liquid crystalline order in polymers. New York: Academic Press; 1978. p. 167–89.
[22] Walker LM, Wagner NJ. Macromolecules 1996;29:2298–301.
[23] Walker LM, Wagner NJ. J Rheol 1995;39:925–52.
[24] Dadmun MD, Muthukumar M, Schwahn D, Springer T. Macromolecules 1996;29:207–11.
[25] Dadmun MD, Muthukumar M, Hempelmann R, Schwahn D, Springer T. J Polym Sci, Part B: Polym Phys 1996;34:649–56.
[26] Chidambaram S, Butler PD, Hamilton WA, Dadmun MD. Scatter Polym 2000;739:356–73.
[27] Dadmun MD, Clingman S, Ober CK, Nakatani AI. J Polym Sci, Part B: Polym Phys 1998;36:3017–23.
[28] He S-J, Lee C, Gido SP, Yu SM, Tirrell DA. Macromolecules 1998; 31:9387–9.
[29] Yu SM, Conticello VP, Zhang G, Kayser C, Fournier MJ, Mason TL, Tirrell DA. Nature 1997;389:167–70.
[30] Toriumi H, Yahagi K, Uematsu I. Mol Cryst Liq Cryst 1983;94: 267–84.
[31] Lecommandoux S, Achard M-F, Langenwalter JF, Klok H-A. Macromolecules 2001;34:9100–11.
[32] Caillol S, Lecommandoux S, Mingotaud A-F, Schappacher M, Soum A, Bryson N, Meyrueix R. Macromolecules 2003;36:1118–24.
[33] Klok HA, Langenwalter JF, Lecommandoux S. Macromolecules 2000;33:7819–26.
[34] Crespo JS, Lecommandoux S, Borsali R, Klok HA, Soldi V. Macromolecules 2003;36:1253–6.
[35] Floudas G, Papadopoulous P, Klok HA, Vandermeulen GWM, Rodriguez-Hernandez J. Macromolecules 2003;36:3673–83.
[36] Fisch MR, Kumar S. Introduction to liquid crystals. In: Kumar S, editor. Liquid crystals: experimental study of physical properties and phase transitions. Cambridge: Cambridge University Press; 2001.
[37] Robinson C. Mol Cryst 1966;1:467–94.
[38] Pierron J, Boudet A, Sopena P. Liq Cryst 1995;19:257–67.
[39] Hara H, Satoh T, Toya T, Iida S, Orii S, Watanabe J. Macromolecules 1998;21:14–19.
[40] Bates FS, Fredrickson GH. Annu Rev Phys Chem 1990;41:525–57.
[41] Almdal K, Mortensen K, Ryan AJ, Bates FS. Macromolecules 1996; 29.
[42] Deming TJ. Macromolecules 1999;32:4500–2.
[43] Nowak AP, Breedveld V, Pakstis L, Ozbas B, Pine DJ, Pochan D, Deming TJ. Nature 2002;417:424–8.
[44] Yu M, Nowak AP, Deming TJ, Pochan D. J Am Chem Soc 1999;121: 12210–1.
[45] Robinson C, Ward JC, Beevers RB. Discuss Faraday Soc 1958; 25:29.
[46] Huang Y, Loos J, Yang YQ, Petermann J. J Polym Sci, Part B: Polym Phys 1998;36:439–45.
[47] Bunning TJ, Vezie DL, Lloyd PF, Haaland PD, Thomas EL, Abrams WW. Liq Cryst 1994;16:769–81.
[48] Boudet A, Mitov M, Bourgerette C, Ondarcuhu T, Coratger R. Ultramicroscopy 2001;88:219–29.
[49] Dong Y, Yuan Q, Huang Y. J Polym Sci, Part B: Polym Phys 2000;38: 980–6.
[50] Gido SP, Thomas EL. Macromolecules 1994;27:6137–44.
[51] Kumar S. Structure: X-ray diffraction studies of liquid crystals. In: Kumar S, editor. Liquid crystals: experimental study of physical properties and phase transitions. Cambridge: Cambridge University Press; 2001.
[52] Samulski E, Tobolski AV. Cholesteric liquid crystals formed by certain polypeptides with organic solvents. In: Gray GW, Windsor PA, editors. Liquid crystals and plastic crystals, vol. I. Chichester: Ellis Horwood Limited; 1974. p. 175–98.
[53] Sartori Blanc N, Senn A, Leforestier A, Livolant F, Dubochet J. J Struct Biol 2001;134:76–81.